First spectroscopic study of ^{63}V at the $N = 40$ island of inversion

M. M. Juhász,[1,2] Z. Elekes,[1] D. Sohler,[1] K. Sieja,[3] K. Yoshida,[4] K. Ogata,[5,6] P. Doornenbal,[7] A. Obertelli,[7,8,9] H. Baba,[7] F. Browne,[7] D. Calvet,[9] F. Château,[9] S. Chen,[7,10,11] N. Chiga,[7] A. Corsi,[9] M. L. Cortés,[7] A. Delbart,[9] J.-M. Gheller,[9] A. Giganon,[9] A. Gillibert,[9] C. Hilaire,[9] T. Isobe,[7] T. Kobayashi,[12] Y. Kubota,[7,13] V. Lapoux,[9] T. Motobayashi,[7] I. Murray,[7,14] H. Otsu,[7] V. Panin,[7] N. Paul,[9] W. Rodriguez,[7,15,16] H. Sakurai,[7,17] M. Sasano,[7] D. Steppenbeck,[7] L. Stuhl,[17,1] Y. L. Sun,[8,9] Y. Togano,[19] T. Uesaka,[7] K. Wimmer,[17,7] K. Yoneda,[7] N. L Achouri,[20] O. Aktas,[21] T. Aumann,[8,22] L. X. Chung,[23] Zs. Dombrádi,[1] F. Flavigny,[14] S. Franchoo,[14] I. Gašparić,[7,24] R.-B. Gerst,[25] J. Gibelin,[20] K. I. Hahn,[26,18] D. Kim,[7,26,18] T. Koiwai,[17] Y. Kondo,[27] P. Koseoglou,[8,22] J. Lee,[11] C. Lehr,[8] B. D. Linh,[23] H. N. Liu,[8,9,21] T. Lokotko,[11] M. MacCormick,[14] K. Moschner,[25] T. Nakamura,[27] S. Y. Park,[28] D. Rossi,[8,22] E. Sahin,[29] P.-A. Söderström,[8,30] S. Takeuchi,[27] H. Törnqvist,[8,22] V. Vaquero,[31] V. Wagner,[8] S. Wang,[32] V. Werner,[8] X. Xu,[11] H. Yamada,[27] D. Yan,[32] Z. Yang,[7] M. Yasuda,[27] and L. Zanetti[8]

[1]*Atomki, Bem tér 18/c., H-4026 Debrecen, Hungary*
[2]*Department of Physics, University of Debrecen, Egyetem tér 1., H-4032 Debrecen, Hungary*
[3]*Université de Strasbourg, CNRS, IPHC UMR 7178, F-67000 Strasbourg, France*
[4]*Advanced Science Research Center, Japan Atomic Energy Agency, Tokai, Ibaraki 319-1195, Japan*
[5]*Research Center for Nuclear Physics (RCNP), Osaka University, Ibaraki 567-0047, Japan*
[6]*Department of Physics, Osaka City University, Osaka 558-8585, Japan*
[7]*RIKEN Nishina Center, 2-1 Hirosawa, Wako, Saitama 351-0198, Japan*
[8]*Institut für Kernphysik, Technische Universität Darmstadt, 64289 Darmstadt, Germany*
[9]*IRFU, CEA, Université Paris-Saclay, F-91191 Gif-sur-Yvette, France*
[10]*State Key Laboratory of Nuclear Physics and Technology, Peking University, Beijing 100871, People' s Republic of China*
[11]*Department of Physics, The University of Hong Kong, Pokfulam Road 17489, Hong Kong*
[12]*Department of Physics, Tohoku University, Sendai 980-8578, Japan*
[13]*Center for Nuclear Study, University of Tokyo, RIKEN campus, Wako, Saitama 351-0198, Japan*
[14]*IJCLab, IN2P3-CNRS, Université Paris-Saclay, 91405 Orsay Cedex, France*
[15]*Universidad Nacional de Colombia, Sede Bogota, Facultad de Ciencias, Departamento de Física, 111321, Bogotá, Colombia*
[16]*Pontificia Universidad Javeriana, Facultad de Ciencias, Departamento de Física, 110231 Bogotá, Colombia*
[17]*Department of Physics, University of Tokyo, 7-3-1 Hongo, Bunkyo, Tokyo 113-0033, Japan*
[18]*Center for Exotic Nuclear Studies, Institute for Basic Science, Daejeon 34126, Korea*
[19]*Department of Physics, Rikkyo University, 3-34-1 Nishi-Ikebukuro, Toshima, Tokyo 172-8501, Japan*
[20]*LPC Caen, ENSICAEN, Université de Caen, CNRS/IN2P3, F-14050 Caen, France*
[21]*Department of Physics, Royal Institute of Technology, SE-10691 Stockholm, Sweden*
[22]*GSI Helmoltzzentrum für Schwerionenforschung GmbH, 64291 Darmstadt, Germany*
[23]*Institute for Nuclear Science and Technology, VINATOM, P.O. Box 5T-160, Nghia Do, Hanoi, Vietnam*
[24]*Ruđer Bošković Institute, Bijenička cesta 54, 10000 Zagreb, Croatia*
[25]*Institut für Kernphysik, Universität zu Köln, D-50937 Cologne, Germany*
[26]*Ewha Womans University, Seoul 03760, Korea*
[27]*Department of Physics, Tokyo Institute of Technology, 2-12-1 O-Okayama, Meguro, Tokyo, 152-8551, Japan*
[28]*Center for Underground Physics, Institute for Basic Science, Daejeon 34126, Korea*
[29]*Department of Physics, University of Oslo, N-0316 Oslo, Norway*
[30]*Extreme Light InfrastructureNuclear Physics (ELI-NP)/Horia Hulubei National Institute for Physics and Nuclear Engineering (IFIN-HH), Str. Reactorului 30, 077125 Bucharest-Măgurele, Romania*
[31]*Instituto de Estructura de la Materia, CSIC, E-28006 Madrid, Spain*
[32]*Institute of Modern Physics, Chinese Academy of Sciences, Lanzhou 730000, China*

(Received 16 February 2021; revised 16 April 2021; accepted 21 May 2021; published 8 June 2021)

The low-lying level structure of ^{63}V was studied for the first time by the inelastic proton scattering and the proton knock-out reaction in inverse kinematics. The comparison of the newly observed γ-ray transitions at 696(8) keV and 889(16) keV with our shell-model calculations using the Lenzi-Nowacki-Poves-Sieja interaction established two excited states proposed to be the first $11/2^-$ and $9/2^-$ levels. The (p, p') excitation cross sections were analyzed by the coupled channel formalism assuming pure quadrupole as well as quadrupole+hexadecapole deformations. This resulted in large deformation parameters placing ^{63}V in the *island of inversion* located below ^{68}Ni.

DOI: 10.1103/PhysRevC.103.064308

I. INTRODUCTION

Studying the mass [1], the magnetic moment [2], and the β decay [3] of the neutron rich sodium isotopes decades ago, some departures from the expectations of the conventional shell model calculations were discovered. The anomalies were theoretically interpreted by introducing an *island of inversion* where the deformation-driven configurations of neutron particle-hole excitations across the $N = 20$ shell gap dominate the ground state of nuclei instead of the spherical, normal configurations [4]. This theoretical work placed only nine nuclei on the island and kept the $N = 20$ shell gap large (around 5 MeV), however it was proposed later that the boundaries of the island should be extended, and the shell gap diminished for these exotic nuclei [5]. Since then numerous experiments as well as theoretical calculations have been carried out (see [6] and references therein), as a result of which, nowadays, we talk about an *archipelago of inversion* located around the neutron numbers 8, 20 28, 40, and 50 with a proposed common underlying mechanism for the reduction of the conventional shell gaps [7].

Regarding the harmonic oscillator shell gap at $N = 40$, a study of iron isotopes [8] indicated the presence of an *island of inversion* twenty years ago. Later on, a theoretical work [9] introduced the Lenzi-Nowacki-Poves-Sieja (LNPS) interaction, and suggested that an *island of inversion* developed in the nuclear chart below ^{68}Ni around $Z = 22$–26 and $N = 38$–42. Here, similar to the *island of inversion* around $N = 20$, the isotopic chains are characterized by open proton shells thus quadrupole correlations can develop. As protons are removed from the $\pi f_{7/2}$ orbit completely filled in ^{68}Ni, the $\nu f_{5/2} - \nu g_{9/2}$ gap gets reduced accompanied by the closeness of the quadrupole partners $\nu g_{9/2}$, $\nu d_{5/2}$ predicting the largest deformation around ^{64}Cr. In the past ten years many experiments have been performed for almost all the isotopic chains below ^{68}Ni toward the dripline including the cobalt [10,11], the iron [12–14], the manganese [15,16], the chromium [17–19], and the titanium [20–22] isotopes. Focusing on the $N = 40$ isotones, by removing protons from ^{68}Ni, the results showed an increase of collectivity up to ^{64}Cr (reaching a quadrupole deformation parameter β_2 of around 0.3 [14]) and a decrease toward the dripline in a good agreement with the theoretical calculations.

However, no experimental data on the nuclear structure of the vanadium isotopes are available around the neutron number 40, only the lifetime of the ground states is known for $N \geqslant 38$ and an isomeric state in ^{64}V [18]. Therefore, we have studied the low-lying excited states of ^{63}V including 40 neutrons by the inelastic proton scattering and the proton knock-out reaction to uncover its deformation and to investigate whether it belongs to the *island of inversion*.

II. EXPERIMENT

The experiment was carried out at the Radioactive Isotope Beam Factory operated by the RIKEN Nishina Center and the Center for Nuclear Study of the University of Tokyo. The accelerator complex provided a beam of ^{70}Zn ions at an energy of 325 MeV/u and at an intensity of 240 pnA. A ^{9}Be production target of 10 mm thickness was placed in the path of the primary beam at the entrance of the BigRIPS separator [23] to fragment the ions. The $B\rho - \Delta E -$ TOF method ($B\rho$: Magnetic rigidity, ΔE: Energy loss, TOF: Time of flight) [24] was applied to select the ions of interest using slits and an aluminum wedged degrader at the first focal plane F1, located between the two dipole magnets D1 and D2 of BigRIPS. The identification of the components in the cocktail beam was done between the focal planes F3 and F7 by time of flight, energy loss and magnetic rigidity measurements. Plastic scintillators at F3 and F7 provided the TOF [25], a gas ionization chamber at F7 [26] determinedthe ΔE, and several sets of parallel plate avalanche counters (PPAC) at F3, F5, and F7 [27,28] monitored the trajectory of the ions. For the vanadium and chromium ions, a 5.5σ separation in Z and a 26.4σ separation in A/Q was achieved. The secondary beam was transported downstream of the focal plane F13 to MINOS [29], a liquid hydrogen target contained in a polyethylene terephthalate cell surrounded by a cylindrical time projection chamber (TPC). The effective target length was determined to be 151(1) mm. The excited states of ^{63}V were populated by the proton inelastic scattering and the proton knock-out reaction which was checked by the correlations of the two protons in their polar and azimuthal angles. The point of reaction was reconstructed either by using the scattered and the removed protons or one of the protons and the projected trajectory of the radioactive ions (the former method was preferred when both data were available) [30]. An overall efficiency of 95% and a resolution of 5 mm (FWHM) along the beam axis was achieved for the events when at least one proton was recorded by the TPC.

An array of 226 NaI(Tl) scintillator crystals (DALI2^{+}) [31,32] placed around the target in cylindrical layers of 10–28 units and a forward wall of 64 units detected the prompt γ rays. Polar angles between 15° and 118° were covered with this arrangement. The beam-like fragments leaving the target were analyzed by the SAMURAI spectrometer [33] based on $B\rho$, ΔE and TOF measurements. The $B\rho$ values were derived via trajectory determination by multiwire drift chambers located upstream (FDC1) and downstream (FDC2) of the magnet operated at a central magnetic field of 2.7 T, using the multidimensional fit procedure of the ROOT framework [34]. Downstream of the FDC2, a plastic scintillator wall consisting of 24 bars yielded the ΔE and TOF information. The unambiguous identification of ^{63}V fragments was ensured by the obtained 8.9σ separation in Z and 7.8σ separation in A/Q. The total beam intensity was approximately 200 particle/s while on average 3/0.4 ^{63}V/^{64}Cr ions hit the liquid hydrogen cell every second. The rate of ^{64}Cr ions was low because they were at the edge of the acceptance of the BigRIPS separator which was tuned to optimize transmission for the primary goal of the experiment, the knock-out reactions ^{53}K$(p, 2p)^{52}$Ar, ^{57}Sc$(p, 2p)^{56}$Ca, and ^{63}V$(p, 2p)^{62}$Ti. The kinetic energy of the ^{63}V and ^{64}Cr particles were around 250 MeV/u at the entrance of the target and the energy loss amounted to about 80 MeV/u while passing through the liquid hydrogen. 2420 and 427 events associated with detected γ rays and an identified proton-track were counted in the inelastic scattering and the proton knock-out reaction channels, respectively.

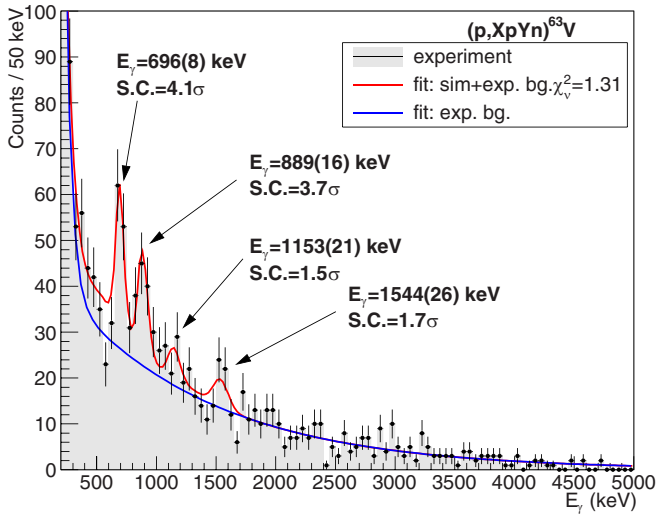

FIG. 1. Doppler corrected γ-ray spectrum for ^{63}V using vertex reconstruction (requiring at least one proton in the TPC) and add-back procedure including all reaction channels. The data with error bars and shaded area represent the experimental spectrum, the red line is the simulation plus a free-parameter double-exponential background, and the latter function (exponential background) is also plotted separately as a blue line. S.C. stands for the statistical confidence of the peaks.

III. RESULTS AND DISCUSSION

Radioactive sources of ^{60}Co, ^{137}Cs and ^{88}Y were used several times during the experiment to calibrate the crystals of the DALI2$^+$ array for energy, thus monitoring the gain shift of the detectors (<0.4%). The photopeak efficiency of the setup was increased by the add-back procedure in the analysis. This procedure merged those hits in the adjacent units (<15 cm) of the DALI2$^+$ array which originated from a single γ ray undergoing Compton-scattering and/or pair production. The γ rays emitted by the fast-moving ions were Doppler-corrected using the vertex position determined by a tracking algorithm for protons in the TPC and the projected trajectory of the ions entering the target. The change of the drift velocity in the TPC was monitored during the experiment and was taken into account in the analysis. In the range of 500–1000 keV the FWHM energy resolution and the add-back photopeak efficiency of the DALI2$^+$ array was around 12% and 35%, respectively. Further details of DALI2$^+$ setup, the Doppler-correction, the add-back procedure as well as the MINOS device and the track reconstruction can be found elsewhere [30–32].

Figure 1 shows the Doppler-corrected γ-ray spectrum for ^{63}V including all the reaction channels indicated by $(p, XpYn)$. The spectrum contains a two-component background: A low-energy part (<500 keV) originating from atomic processes and a high-energy part coming from other sources mainly the reactions of the scattered particles on the materials surrounding the target [35,36]. This background was modeled by a double-exponential function with four free parameters which proved to be successful for other reactions of this experiment [21,37–40] as well as for our earlier similar experiments [19,36,41–46]. The spectrum clearly shows two peaks at around 700 keV and 900 keV and some other candidates at higher energies. In order to determine the statistical confidence, the energy and the intensity of these peaks a simulation was performed by a GEANT4 [47] application especially developed for our SUNFLOWER collaboration [48]. This application could provide the response function of the DALI2$^+$ setup for a γ ray emitted by the fast-moving projectile taking into account the intrinsic experimental resolution of the NaI(Tl) detectors. The resulting response functions were added together with individual scaling parameters plus the double-exponential function to fit the spectrum using the likelihood method [49] of the ROOT framework [50], which gave more reliable results for the spectra with low statistics [37,51]. The total fit with a reduced χ^2 (χ^2_ν) of 1.31 is presented by a red line in Fig. 1 while the background is plotted by a blue line. The energy of the four most prominent peaks shown in the figure were obtained to be 696(8) keV, 889(16) keV, 1153(21) keV, and 1544(26) keV. The statistical confidence of the latter two peaks were determined to be very low (1.5σ, 1.7σ, respectively), and it reached the 3σ limit of unambiguous existence for only the first two peaks (4.1σ, 3.7σ, respectively). For the other peak candidates at higher energies, the statistical confidence was lower than the smallest quoted one. Indeed, by including only the 696-keV and the 889-keV peaks in the fit, a $\chi^2_\nu = 1.41$ value could be obtained, which means there is no need to assume any other peaks to correctly describe the spectrum. The stability of the statistical significance of the peaks were also checked using smaller bin sizes of 40 keV, 30 keV, and 20 keV: The values for the 696-keV and the 889-keV peaks remained above 3.7σ and 3.5σ, respectively while the values for the other peak candidates stayed below 2.0σ. The dependence of the peak parameters and of the fit quality on the background was also investigated in a similar manner described in our previous work where the spectrum statistics was close to the present one [37]: Instead of the free-parameter double-exponential function we took the background shape extracted from a high-statistics spectrum of ^{61}V, a nucleus close to the studied one. This analysis gave a slightly higher χ^2_ν of 1.39 including the four most prominent peaks in the fit. Again, only the 696-keV and the 889-keV peaks showed statistical confidences of 4.8σ and 4.1σ above the 3σ limit, respectively. The quoted uncertainties for the energy of the γ rays originated from the statistics, the energy calibration (5 keV), and the background estimation. The low statistics did not allow us to perform a $\gamma\gamma$ analysis of the events, so no primary conclusion could be drawn on whether the observed transitions were parallel or cascade.

The spectra for the individual reaction channels of (p, p') (upper panel) and $(p, 2p)$ (lower panel) in Fig. 2 were analyzed in the same way as the $(p, XpYn)$ spectrum. The only exception was that not only the background from the $(p, XpYn)$ spectrum of ^{61}V but also that of the ^{61}V$(p, p')^{61}$V and the ^{62}V$(p, pn)^{61}$V high-statistics spectra were considered for the ^{63}V$(p, p')^{63}$V and ^{64}Cr$(p, 2p)^{63}$V reactions, respectively. The fits shown in the panels of Fig. 2 include the most prominent peaks. According to the analysis the 696-keV and the 889-keV transitions for the inelastic channel and only the 696-keV peak for the knock-out channel could be proved

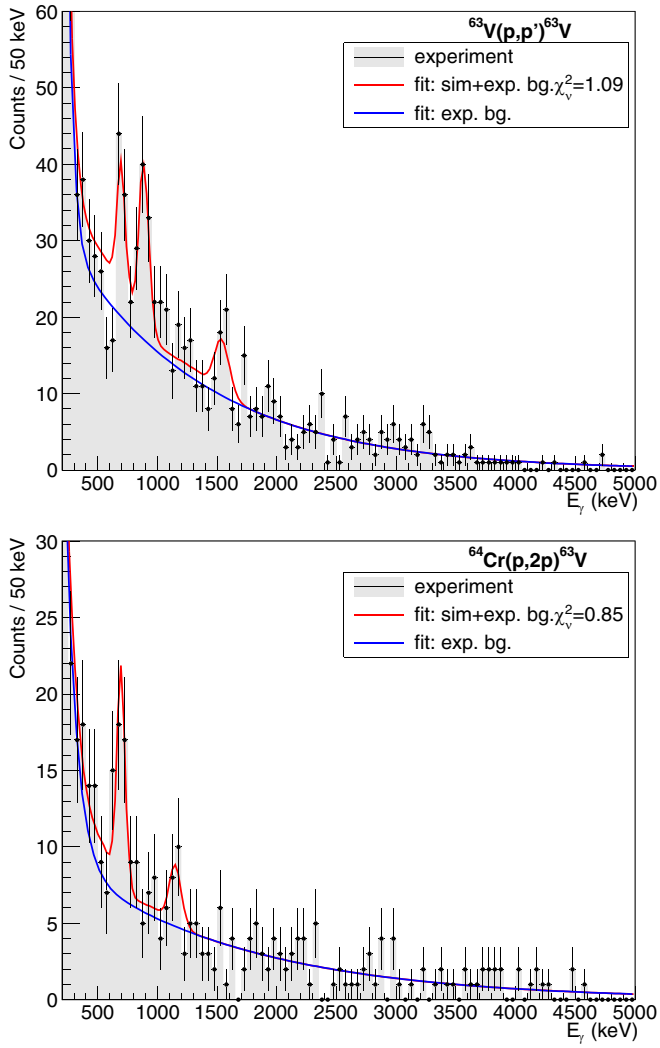

FIG. 2. Doppler corrected γ-ray spectra for ^{63}V using vertex reconstruction (requiring at least one proton in the TPC) and add-back procedure [upper panel: Inelastic scattering, lower panel: ^{64}Cr$(p, 2p)^{63}$V reaction channel]. The data with error bars and shaded area represent the experimental spectrum, the red line is the simulation plus a free-parameter double-exponential background, and the latter function (exponential background) is also plotted separately as a blue line.

to exist above the 3σ limit. It is noted that 96.8% of the events in the inelastic channel were associated with the expected one-proton track in the MINOS device. For the $(p, 2p)$ reaction, two-proton-track events dominated with 78.9% as expected while the percentage of the one-proton-track events was 20.5%. Analyzing only the one-proton-track events for the (p, p') reaction and the two-proton-track events for the $(p, 2p)$ reaction we again arrived to the above conclusion regarding the existence of the transitions.

Based on the observed number of γ rays and that of the incoming ions, a γ-ray-production cross section of $\sigma(p2p; 696\gamma\downarrow) = 1.0(3)$ mb associated with the 696-keV transition in the $(p, 2p)$ channel while γ-ray-production cross sections of $\sigma(pp'; 696\gamma\downarrow) = 0.14(6)$ mb and $\sigma(pp'; 889\gamma\downarrow) = 0.24(7)$ mb for the inelastic scattering were determined. The uncertainties are dominated by the statistical uncertainty originating from the fits but they also include quadratically the other contributions coming from the choice of the background, the simulated photopeak efficiency of the DALI2$^+$ array and the target thickness. The inclusive cross section for the $(p, 2p)$ channel was extracted to be 8.7(4) mbarn.

IV. COMPARISON TO THEORY

In order to interpret the observed data, large scale shell model calculations were performed to determine the low-energy level and decay scheme of ^{63}V and to describe the proton knock-out reaction. The calculated spectroscopic factors for the $(p, 2p)$ reaction were combined with the single-particle cross sections calculated in the distorted wave impulse approximation (DWIA) framework to derive the theoretical $(p, 2p)$ cross sections. For the inelastic scattering, a coupled channel calculation was performed to determine the deformation of ^{63}V.

a. Shell model calculation. The details of the shell-model calculation were described earlier [9]. The valence space comprised of neutron $(f_{5/2}p_{3/2}p_{1/2}g_{9/2}d_{5/2})$ and proton *fp* orbitals. The Hamiltonian was based on the LNPS interaction. Due to the large size of the configuration space, the calculations were truncated to 10p-10h excitations across $Z = 28$ and $N = 40$ gaps, which assured, however, a good convergence of the calculated spectra. The diagonalization of the Hamiltonian matrices was done by the Strasbourg shell-model code ANTOINE [52,53]. To get the theoretical branching ratios, the $E2/M1$ reduced transition rates were obtained using effective charges $e_p = 1.31$, $e_n = 0.46$ for $B(E2)$ and $g_l^n = 0.0$, $g_s^n = -2.87$, $g_l^p = 1.0$, $g_s^p = 4.19$ for the $B(M1)$ values [53,54]. The standard effective charges ($e_p = 1.5$, $e_n = 0.5$) overestimated the $B(E2)$ values for neutron rich chromium and iron isotopes [55], however, the present framework with the modified effective charges deduced theoretically in Ref. [54], proved to be very powerful interpreting the experimental results around the $N = 40$ shell gap in the past ten years: (a) $E(2_1^+)$, $B(E2)$ for the neutron rich chromium and iron isotopic chains [14], (b) low-energy level scheme of ^{58,60}Ti within 100 keV [20], (c) $E(2_1^+)$, $E(2_1^+)/E(4_1^+)$ for the neutron rich chromium and iron isotopic chains [19], (d) low-energy level scheme of ^{53,55,57}Mn within 100 keV [16], (e) $B(E2)$ for ^{72,74}Ni [36], (f) low-energy level scheme of ^{62}Ti within 100 keV [21]. It is worth emphasizing that the calculated $B(E2; 2_1^+ \rightarrow 0_1^+)$ values for the experimentally studied $N = 40$ nuclei (^{68}Ni: 41 e^2fm^4, ^{66}Fe: 336 e^2 fm^4, ^{64}Cr: 361 e^2fm^4) are very similar to the observed values of 53(6) e^2fm^4, 299(17) e^2fm^4, and 312(79) e^2fm^4 [14,56–59].

b. DWIA. The distorted wave impulse approximation framework was thoroughly discussed elsewhere [60]. Since the $(p, 2p)$ reaction took place in a long (151 mm) target, the single-particle cross sections calculated at different energies were averaged over the energy range corresponding to the target length weighting the cross section values with the observed statistics, as it was done in our earlier works (e.g., [37,40,61]).

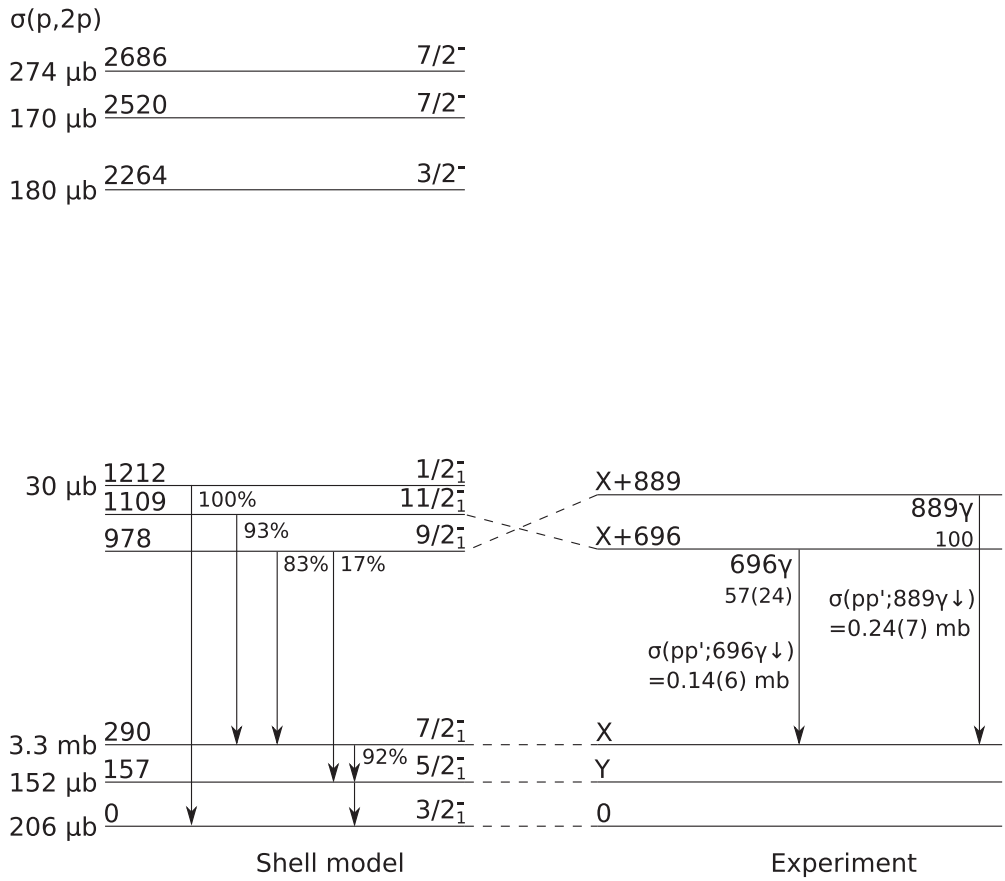

FIG. 3. Partial level and decay scheme of ^{63}V. The two observed bound excited states with their decay and relative γ-ray intensities in the (p,p') channel are shown on the right hand side as well as the experimental γ-ray-production cross sections for the inelastic scattering next to the arrows. The experimental data were compared with our shell-model calculations on the left-hand side. The calculated γ-ray branching ratios are also written next to the downward arrows. Both experimental transitions could be matched with counterparts in the shell-model level scheme. The $(p, 2p)$ cross section values left-hand side of the theoretical levels were derived from the spectroscopic factors and the theoretical single-particle cross sections. Only those states are displayed above the $1/2^-_1$ one and below the neutron separation energy of 4.7(13) MeV [22] (mass systematics: 4.6 MeV [62]), for which the calculated $(p, 2p)$ cross section is above 0.1 mb. There are around 40 other states above the $1/2^-_1$ one which were calculated to be populated in the knock-out reaction with very small spectroscopic factors.

c. Coupled channel calculation. The coupled channel calculation was performed by the ECIS code [63] using the symmetric rotational model. The standard collective form factors were applied together with the optical potential parameters determined from the global phenomenological set of Koning and Delaroche [64] which was successfully used, e.g., in the analysis of a similar experiment for Ni and Zn isotopes [36]. The model parameters of the quadrupole matter (δ_2^M) and Coulomb deformation lengths (δ_2^C) were kept equal, which is a usual approach since the proton and neutron distributions do not differ significantly for wide range of nuclei [65–67].

d. Interpretation of the experimental data. The partial level and decay scheme from the shell model is presented on the left-hand side of Fig. 3 together with the calculated $(p, 2p)$ cross sections. The ground state is calculated to be $3/2^-$, which was found to be consistent with the non-observation of the population of the 4^+_1 state in ^{62}Cr following β-delayed neutron emission [68], as well as the number of states populated in the ^{63}V$(p, 2p)^{62}$Ti knock-out reaction [21]. Also, the LNPS calculation provided the $3/2^-$ ground state for ^{61}V in line with the β-decay [69] and the knock-out data [20]. Therefore, the $3/2^-$ ground state is a realistic starting point for the interpretation of the experimental results.

Since the (p, p') reaction usually populates the lowest-energy levels strongly coupled to the ground state, the lowest few excited states (which are the first calculated levels for each spin up to $11/2$) are shown in Fig. 3. According to our calculation only three of these states (including the ground state) and three other states at higher energies (2264 keV, 2520 keV, 2686 keV) are expected to be populated with significant cross sections (>0.1 mb) by the $(p, 2p)$ reaction. Therefore, the 40 other states calculated between the 1212-keV level and the one-neutron separation energy of 4.7(13) MeV [22] are not plotted.

^{63}V is located on the $N = 40$ isotonic chain between ^{64}Cr and ^{62}Ti, which were experimentally suggested to belong to the *island of inversion* with large quadrupole deformation parameters of around $\beta_2 = 0.3$ [14,21]. With this typical β_2

value, our coupled channel calculation gives (p, p') excitation cross sections of 5.7 mb and 3.3 mb for the calculated $5/2_1^-$ and the $7/2_1^-$ levels, respectively. Even with half of this β_2 value usual in the *island of inversion*, the calculated cross sections are about an order of magnitude larger than the observed $\sigma(pp'; 696\gamma\downarrow) = 0.15(6)$ mb and $\sigma(pp'; 889\gamma\downarrow) = 0.24(7)$ mb values. It is noted that the dependence of the calculated cross sections on the energy of the levels is negligible at this low-energy regime. Therefore, we can conclude that the γ rays observed in the (p, p') reaction cannot be associated with the excitation of the $5/2_1^-$ and the $7/2_1^-$ levels, which is also supported by the large energy difference between the expected γ rays of around 150 keV (emitted by the de-exciting $5/2_1^-$ and the $7/2_1^-$ levels) and the experimental ones (696 keV, 889 keV). Similar cross-section arguments hold for the calculated $1/2_1^-$ level at 1212 keV and others with spin $J \leqslant 7/2$ due to $J_{GS} = 3/2$.

However, the theoretical $9/2_1^-$ and $11/2_1^-$ levels seem to be very good candidates for the assignment of the γ rays observed in the (p, p') reaction. Both of them predominantly decay to the $7/2_1^-$ level with transition energies of 688 keV and 819 keV, which are close to the experimental values. Also, due to their spin/parity they are expected to be weakly excited in the (p, p') reaction, which also coincides with the observation. The experimental production cross section of the 889-keV γ ray is larger than that of the 696-keV γ ray, which suggest that the former can be assigned to the excitation of the $9/2_1^-$ level, while the latter belongs to excitation of the $11/2_1^-$ level. Indeed, with a quadrupole deformation length parameter of $\delta_2 = \delta_2^M = \delta_2^C = 2.25(22)$ fm, the coupled channel calculation could reproduce the (p, p') excitation cross sections of $\sigma(9/2_1^-; X + 889\uparrow)$=0.29(9) mb and $\sigma(11/2_1^-; X+696\uparrow) =$ 0.15(6) mb taking into account the calculated γ-ray branching ratios of the $9/2_1^-$ (83%) and the $11/2_1^-$ (93%) levels. The derived δ_2 corresponds to the quadrupole deformation parameter $\beta_2 = 0.47(5)$ with the well-known relation $\delta_i = \beta_i\, 1.2\,\text{fm}\, A^{1/3}$. The quoted uncertainty originates from the uncertainty of the observed cross section. However, it is worth noting that the choice of the optical potential usually adds about 10% uncertainty to the deformation parameter [36,70].

This analysis implied multistep excitations of the $9/2_1^-$ and $11/2_1^-$ states through the $5/2_1^-$ and $7/2_1^-$ states. However, additional single-step excitations can also be expected in the inelastic scattering which in turn might reduce δ_2 and can be handled by introducing hexadecapole deformation length parameter δ_4 in the ECIS calculations beside the quadrupole deformation length parameter δ_2. This higher order deformation is usually small in most of the nuclei compared to the quadrupole deformation expected from calculations based on the finite-range droplet macroscopic and the folded-Yukawa single-particle microscopic nuclear structure models [71]. Due to its small value, it is difficult to measure, and so experimental values are only available for rare-earth isotopes [72], actinides [73], and some stable light nuclei [74,75]. For exotic nuclei, the measurements are even more scarce, yet, δ_4/δ_2 was determined to be 0.27(5) for ^{32}Mg lying in the *island of inversion* around $N = 20$ [76]. The angular distribution for the excitation of the 4_1^+ state could only be reproduced by this hexadecapole deformation therefore it is not surprising that our analysis with pure quadrupole deformation resulted in such a high δ_2 value (2.25 fm). Using the upper limit of the value $\delta_4/\delta_2 = 1/3$ in Ref. [76], the ECIS calculation provides $\delta_2 = 1.14(12)$ fm and $\delta_4 = 0.38(4)$ fm corresponding to $\beta_2 = 0.24(2)$ and $\beta_4 = 0.08(1)$. The shell model calculation gives $\delta_2 = 1.39$ fm ($\beta_2 = 0.29$), agreeing with the experimental value assuming realistic higher-order excitations, which also supports the expounded assignment of the experimental transitions.

Regarding the $(p, 2p)$ channel, if we add the calculated cross sections up to the estimated neutron separation energy of 4.6 MeV for ^{63}V, we end up with 6.1 mb, which is fairly close to the experimental inclusive cross section of 8.7(4) mb. Nevertheless, the origin of one of the two γ rays (696 keV) in the $(p, 2p)$ channel with a γ-ray-production cross section of $\sigma(p2p; 696\gamma\downarrow) = 1.0(3)$ mb is not straightforward. Based on the calculated $(p, 2p)$ cross sections the only possibility of a direct production is the population of the $7/2_1^-$ level at 290 keV. However, the energy difference (696 keV vs. $\approx$150 keV) would be very large for the experimental and theoretical values. Furthermore, this assignment is in conflict with the observation in the (p, p') reaction. But, if we assume the assignment from the analysis of the (p, p') reaction (i.e., the 696-keV γ ray is produced by the de-excitation of the $11/2_1^-$ state), there are three calculated levels (2264-keV, 2520-keV, 2686-keV) above the $11/2_1^-$ level populated with significant cross sections (180 μb, 174μb, 274 μb, respectively) in the $(p, 2p)$ reaction. Although there are numerous (about 20) other states between these three levels and the $11/2_1^-$ level, and thus it is difficult to map their decay pattern, it is possible that the 696-keV γ ray is produced after cascade decays of the three high-lying states. On the other hand, it could also happen that the $11/2_1^-$ level was populated in two steps via ^{64}Cr$(p, p')\,^{64}$Cr$^{2+}(p, 2p)\,^{63}$V or by nonsudden dissipative process [77] as in our earlier experiment [16].

In summary, both the (p, p') and the $(p, 2p)$ reactions can be interpreted by the most plausible level scheme plotted on the right side of Fig. 3, and a large quadrupole deformation parameter ($\beta_2 > 0.22$) can be assigned to ^{63}V, suggesting that this nucleus belongs to the *island of inversion* below ^{68}Ni.

V. SUMMARY

The low-lying excited states of ^{63}V unexplored so far were investigated by the inelastic scattering and the proton knock-out reaction. For the first time, two γ rays were detected in the Doppler-corrected spectrum for the (p, p') reaction at energies of 696(8) keV and 889(16) keV, while only the lower-energy transition was observed in the $(p, 2p)$ channel. The experimental data were compared to our shell-model calculations using the LNPS interaction, and as a result two excited states proposed to be the first $11/2^-$ and $9/2^-$ levels were established decaying to the unobserved $7/2_1^-$ level. Analyzing the excitation cross section of these two excited states in the (p, p') reaction using multistep and single-step excitations with realistic $\delta_4/\delta_2 = 1/3$ ratio by the coupled channel formalism, the quadrupole and hexadecapole matter and Coulomb deformation length parameters of $\delta_2 =$

$\delta_2^M = \delta_2^C = 1.14(12)$ fm, $\delta_4 = \delta_4^M = \delta_4^C = 0.38(4)$ fm were obtained, which corresponds to quadrupole and hexadecapole deformation parameters of $\beta_2 = 0.24(2)$, $\beta_4 = 0.08(1)$. This large β_2 deformation parameter was found to be in a good agreement with the shell model calculations, thus ^{63}V could be placed in the *island of inversion* below ^{68}Ni.

ACKNOWLEDGMENTS

We are very grateful to the RIKEN Nishina Center accelerator staff for providing the stable beam and to the BigRIPS team for the smooth operation of the secondary beams. The development of the MINOS device has been supported by the European Research Council through the ERC Grant No. MINOS-258567. F.B. was supported by the RIKEN Special Postdoctoral Researcher Program. K.O. acknowledges the support by Grant-in-Aid for Scientific Research JP16K05352. Y.U. acknowledges the support by Grant-in-Aid for Scientific Research No. 20K03981. Y.L.S. acknowledges the support of Marie Skłodowska-Curie Individual Fellowship (H2020-MSCA-IF-2015-705023) from the European Union and the support from the Helmholtz International Center for FAIR. H.N.L. acknowledges the support from the Enhanced Eurotalents program (PCOFUND-GA-2013-600382) co-funded by CEA and the European Union. T.A., C.L., D.R., H.T., V.W., L.Z., H.N.L., V.W., and A.O. acknowledge the support from the Deutsche Forschungsgemeinschaft (DFG, German Research Foundation) Project No. 279384907-SFB 1245. R.B.G. acknowledges the support from the DFG under Grant No. BL 1513/1-1. Y.L.S. and A.O. acknowledge the support from the Alexander von Humboldt Foundation. B.D.L. and L.X.C. acknowledge the support from the Vietnam Ministry of Science and Technology under Grant No. ĐTCB.01/21/VKHKTHN. I.G. has been supported by HIC for FAIR and HRZZ under Projects No. 1257 and No. 7194. F.B. acknowledge the support from the RIKEN Special Postdoctoral Researcher Program. D.S. and Z.E. were supported by Projects No. GINOP-2.3.3-15-2016-00034 and K128947. V.V. acknowledges support from the Spanish Ministerio de Economía y Competitividad under Contract No. FPA2017-84756-C4-2-P. V.W. and P.K. acknowledge the support from BMBF Grants No. 05P15RDFN1 and No. 05P19RDFN1. P.K. acknowledges support from HGS-HIRe. This work was also supported by NKFIH (114454) and by Swedish Research Council under Grants No. 621-2014-5558 and No. 2019-04880. K.I.H., D.K., and S.Y.P. acknowledge the support from the IBS grant funded by the Korea government (No. IBS-R031-D1). T.N. and Y.K. acknowledge the support by JSPS Grant-in-Aid for Scientific Research Grants No. JP16H02179, No. JP18H05404, and No. JP21H04465.

[1] C. Thibault, R. Klapisch, C. Rigaud, A. M. Poskanzer, R. Prieels, L. Lessard, and W. Reisdorf, Phys. Rev. C **12**, 644 (1975).
[2] G. Huber, F. Touchard, S. Büttgenbach, C. Thibault, R. Klapisch, H. T. Duong, S. Liberman, J. Pinard, J. L. Vialle, P. Juncar *et al.*, Phys. Rev. C **18**, 2342 (1978).
[3] C. Détraz, D. Guillemaud, G. Huber, R. Klapisch, M. Langevin, F. Naulin, C. Thibault, L. C. Carraz, and F. Touchard, Phys. Rev. C **19**, 164 (1979).
[4] E. K. Warburton, J. A. Becker, and B. A. Brown, Phys. Rev. C **41**, 1147 (1990).
[5] Y. Utsuno, T. Otsuka, T. Mizusaki, and M. Honma, Phys. Rev. C **60**, 054315 (1999).
[6] T. Otsuka, A. Gade, O. Sorlin, T. Suzuki, and Y. Utsuno, Rev. Mod. Phys. **92**, 015002 (2020).
[7] F. Nowacki and A. Poves, J. Phys.: Conf. Ser. **966**, 012023 (2018).
[8] M. Hannawald, T. Kautzsch, A. Wöhr, W. B. Walters, K.-L. Kratz, V. N. Fedoseyev, V. I. Mishin, W. Böhmer, B. Pfeiffer, V. Sebastian *et al.*, Phys. Rev. Lett. **82**, 1391 (1999).
[9] S. M. Lenzi, F. Nowacki, A. Poves, and K. Sieja, Phys. Rev. C **82**, 054301 (2010).
[10] F. Recchia, S. M. Lenzi, S. Lunardi, E. Farnea, A. Gadea, N. Mărginean, D. R. Napoli, F. Nowacki, A. Poves, J. J. Valiente-Dobón *et al.*, Phys. Rev. C **85**, 064305 (2012).
[11] L. Canete, S. Giraud, A. Kankainen, B. Bastin, F. Nowacki, A. Poves, P. Ascher, T. Eronen, V. Alcindor, A. Jokinen, A. Khanam, I. D. Moore, D. A. Nesterenko, F. De Oliveira Santos, H. Penttila, C. Petrone, I. Pohjalainen, A. de Roubin, V. A. Rubchenya, M. Vilen, and J. Aysto, Phys. Rev. C **101**, 041304(R) (2020).
[12] J. Ljungvall, A. Görgen, A. Obertelli, W. Korten, E. Clément, G. deFrance, A. Bürger, J. P. Delaroche, A. Dewald, A. Gadea, L. Gaudefroy, M. Girod, M. Hackstein, J. Libert, D. Mengoni, F. Nowacki, T. Pissulla, A. Poves, F. Recchia, M. Rejmund, W. Rother, E. Sahin, C. Schmitt, A. Shrivastava, K. Sieja, J. J. Valiente-Dobon, K. O. Zell, and M. Zielinska, Phys. Rev. C **81**, 061301(R) (2010).
[13] S. Naimi, G. Audi, D. Beck, K. Blaum, C. Böhm, C. Borgmann, M. Breitenfeldt, S. George, F. Herfurth, A. Herlert *et al.*, Phys. Rev. C **86**, 014325 (2012).
[14] H. L. Crawford, R. M. Clark, P. Fallon, A. O. Macchiavelli, T. Baugher, D. Bazin, C. W. Beausang, J. S. Berryman, D. L. Bleuel, C. M. Campbell *et al.*, Phys. Rev. Lett. **110**, 242701 (2013).
[15] S. N. Liddick, S. Suchyta, B. Abromeit, A. Ayres, A. Bey, C. R. Bingham, M. Bolla, M. P. Carpenter, L. Cartegni, C. J. Chiara, H. L. Crawford, I. G. Darby, R. Grzywacz, G. Gurdal, S. Ilyushkin, N. Larson, M. Madurga, E. A. McCutchan, D. Miller, S. Padgett, S. V. Paulauskas, J. Pereira, M. M. Rajabali, K. Rykaczewski, S. Vinnikova, W. B. Walters, and S. Zhu, Phys. Rev. C **84**, 061305(R) (2011).
[16] X. Liu, Z. Liu, B. Ding, P. Doornenbal, A. Obertelli, S. Lenzi, P. Walker, L. Chung, B. Linh, G. Authelet *et al.*, Phys. Lett. B **784**, 392 (2018).
[17] A. Gade, R. V. F. Janssens, T. Baugher, D. Bazin, B. A. Brown, M. P. Carpenter, C. J. Chiara, A. N. Deacon, S. J. Freeman, G. F. Grinyer, C. R. Hoffman, B. P. Kay, F. G. Kondev, T. Lauritsen, S. McDaniel, K. Meierbachtol, A. Ratkiewicz, S. R. Stroberg,

K. A. Walsh, D. Weisshaar, R. Winkler, and S. Zhu, Phys. Rev. C **81**, 051304(R) (2010).
[18] S. Suchyta, S. N. Liddick, C. J. Chiara, W. B. Walters, M. P. Carpenter, H. L. Crawford, G. F. Grinyer, G. Gürdal, A. Klose, E. A. McCutchan *et al.*, Phys. Rev. C **89**, 067303 (2014).
[19] C. Santamaria, C. Louchart, A. Obertelli, V. Werner, P. Doornenbal, F. Nowacki, G. Authelet, H. Baba, D. Calvet, F. Château *et al.*, Phys. Rev. Lett. **115**, 192501 (2015).
[20] A. Gade, R. V. F. Janssens, D. Weisshaar, B. A. Brown, E. Lunderberg, M. Albers, V. M. Bader, T. Baugher, D. Bazin, J. S. Berryman *et al.*, Phys. Rev. Lett. **112**, 112503 (2014).
[21] M. Cortés, W. Rodriguez, P. Doornenbal, A. Obertelli, J. Holt, S. Lenzi, J. Menéndez, F. Nowacki, K. Ogata, A. Poves *et al.*, Phys. Lett. B **800**, 135071 (2020).
[22] S. Michimasa, M. Kobayashi, Y. Kiyokawa, S. Ota, R. Yokoyama, D. Nishimura, D. S. Ahn, H. Baba, G. P. A. Berg, M. Dozono *et al.*, Phys. Rev. Lett. **125**, 122501 (2020).
[23] T. Kubo, D. Kameda, H. Suzuki, N. Fukuda, H. Takeda, Y. Yanagisawa, M. Ohtake, K. Kusaka, K. Yoshida, N. Inabe *et al.*, Prog. Theor. Exp. Phys. **2012** (2012), 03C003.
[24] T. Kubo, Nucl. Instrum. Methods Phys. Res. B **204**, 97 (2003), 14th International Conference on Electromagnetic Isotope Separators and Techniques Related to their Applications.
[25] N. Fukuda, T. Kubo, T. Ohnishi, N. Inabe, H. Takeda, D. Kameda, and H. Suzuki, Nucl. Instrum. Methods Phys. Res. B **317**, 323 (2013).
[26] K. Kimura, T. Izumikawa, R. Koyama, T. Ohnishi, T. Ohtsubo, A. Ozawa, W. Shinozaki, T. Suzuki, M. Takahashi, I. Tanihata *et al.*, Nucl. Instrum. Methods Phys. Res. A **538**, 608 (2005).
[27] H. Kumagai, A. Ozawa, N. Fukuda, K. Sümmerer, and I. Tanihata, Nucl. Instrum. Methods Phys. Res. A **470**, 562 (2001).
[28] H. Kumagai, T. Ohnishi, N. Fukuda, H. Takeda, D. Kameda, N. Inabe, K. Yoshida, and T. Kubo, Nucl. Instrum. Methods Phys. Res. B **317**, 717 (2013).
[29] A. Obertelli, A. Delbart, S. Anvar, L. Audirac, G. Authelet, H. Baba, B. Bruyneel, D. Calvet, F. Château, A. Corsi *et al.*, Eur. Phys. J. A **50**, 8 (2014).
[30] C. Santamaria, A. Obertelli, S. Ota, M. Sasano, E. Takada, L. Audirac, H. Baba, D. Calvet, F. Château, A. Corsi *et al.*, Nucl. Instrum. Methods Phys. Res. A **905**, 138 (2018).
[31] S. Takeuchi, T. Motobayashi, Y. Togano, M. Matsushita, N. Aoi, K. Demichi, H. Hasegawa, and H. Murakami, Nucl. Instrum. Methods Phys. Res. A **763**, 596 (2014).
[32] I. Murray, F. Browne, S. Chen, M. L. Cortés, P. Doornenbal, H. Sakurai, J. Lee, M. MacCormick, W. Rodriguez, V. Vaquero *et al.*, RIKEN Accelerator Progress Report **51**, 158 (2018).
[33] T. Kobayashi, N. Chiga, T. Isobe, Y. Kondo, T. Kubo, K. Kusaka, T. Motobayashi, T. Nakamura, J. Ohnishi, H. Okuno *et al.*, Nucl. Instrum. Methods Phys. Res. B **317**, 294 (2013), XVIth International Conference on ElectroMagnetic Isotope Separators and Techniques Related to their Applications, December 2–7, 2012 at Matsue, Japan.
[34] ROOT MultiDimFit (accessed March 29, 2021), https://root.cern.ch/doc/master/classTMultiDimFit.html.
[35] P. Doornenbal, Prog. Theor. Exp. Phys. **2012**, 03C004 (2012).
[36] M. L. Cortés, P. Doornenbal, M. Dupuis, S. M. Lenzi, F. Nowacki, A. Obertelli, S. Péru, N. Pietralla, V. Werner, K. Wimmer *et al.*, Phys. Rev. C **97**, 044315 (2018).
[37] H. N. Liu, A. Obertelli, P. Doornenbal, C. A. Bertulani, G. Hagen, J. D. Holt, G. R. Jansen, T. D. Morris, A. Schwenk, R. Stroberg *et al.*, Phys. Rev. Lett. **122**, 072502 (2019).
[38] Y. Sun, A. Obertelli, P. Doornenbal, C. Barbieri, Y. Chazono, T. Duguet, H. Liu, P. Navrátil, F. Nowacki, K. Ogata *et al.*, Phys. Lett. B **802**, 135215 (2020).
[39] M. L. Cortés, W. Rodriguez, P. Doornenbal, A. Obertelli, J. D. Holt, J. Menéndez, K. Ogata, A. Schwenk, N. Shimizu, J. Simonis *et al.*, Phys. Rev. C **102**, 064320 (2020).
[40] M. Juhász, Z. Elekes, D. Sohler, Y. Utsuno, K. Yoshida, T. Otsuka, K. Ogata, P. Doornenbal, A. Obertelli, H. Baba *et al.*, Phys. Lett. B **814**, 136108 (2021).
[41] S. Chen, P. Doornenbal, A. Obertelli, T. R. Rodríguez, G. Authelet, H. Baba, D. Calvet, F. Château, A. Corsi, A. Delbart *et al.*, Phys. Rev. C **95**, 041302(R) (2017).
[42] F. Flavigny, P. Doornenbal, A. Obertelli, J.-P. Delaroche, M. Girod, J. Libert, T. R. Rodriguez, G. Authelet, H. Baba, D. Calvet *et al.*, Phys. Rev. Lett. **118**, 242501 (2017).
[43] M. Lettmann, V. Werner, N. Pietralla, P. Doornenbal, A. Obertelli, T. R. Rodríguez, K. Sieja, G. Authelet, H. Baba, D. Calvet *et al.*, Phys. Rev. C **96**, 011301(R) (2017).
[44] T. Lokotko, S. Leblond, J. Lee, P. Doornenbal, A. Obertelli, A. Poves, F. Nowacki, K. Ogata, K. Yoshida, G. Authelet *et al.*, Phys. Rev. C **101**, 034314 (2020).
[45] L. Olivier, S. Franchoo, M. Niikura, Z. Vajta, D. Sohler, P. Doornenbal, A. Obertelli, Y. Tsunoda, T. Otsuka, G. Authelet *et al.*, Phys. Rev. Lett. **119**, 192501 (2017).
[46] C. Shand, Z. Podolyák, M. Górska, P. Doornenbal, A. Obertelli, F. Nowacki, T. Otsuka, K. Sieja, J. Tostevin, Y. Tsunoda *et al.*, Phys. Lett. B **773**, 492 (2017).
[47] S. Agostinelli, J. Allison, K. Amako, J. Apostolakis, H. Araujo, P. Arce, M. Asai, D. Axen, S. Banerjee, G. Barrand *et al.*, Nucl. Instrum. Methods Phys. Res. A **506**, 250 (2003).
[48] SUNFLOWER collaboration (accessed March 29, 2021), https://www.nishina.riken.jp/collaboration/SUNFLOWER/misc/download/simulation.php.
[49] S. Baker and R. D. Cousins, Nucl. Instrum. Methods Phys. Res. **221**, 437 (1984).
[50] I. Antcheva, M. Ballintijn, B. Bellenot, M. Biskup, R. Brun, N. Buncic, P. Canal, D. Casadei, O. Couet, V. Fine *et al.*, Comput. Phys. Commun. **180**, 2499 (2009).
[51] Nuclear structure in the vicinity of ^{78}Ni: In-beam gamma-ray spectroscopy of ^{79}Cu through proton knockout (accessed March 29, 2021), https://tel.archives-ouvertes.fr/tel-01637435/document.
[52] F. Nowacki and E. Caurier, Acta Phys. Polo. B **30**, 749 (1999).
[53] E. Caurier, G. Martínez-Pinedo, F. Nowack, A. Poves, and A. P. Zuker, Rev. Mod. Phys. **77**, 427 (2005).
[54] M. Dufour and A. P. Zuker, Phys. Rev. C **54**, 1641 (1996).
[55] T. Baugher, A. Gade, R. V. F. Janssens, S. M. Lenzi, D. Bazin, B. A. Brown, M. P. Carpenter, A. N. Deacon, S. J. Freeman, T. Glasmacher, G. F. Grinyer, F. G. Kondev, S. McDaniel, A. Poves, A. Ratkiewicz, E. A. McCutchan, D. K. Sharp, I. Stefanescu, K. A. Walsh, D. Weisshaar, and S. Zhu, Phys. Rev. C **86**, 011305(R) (2012).
[56] O. Sorlin, S. Leenhardt, C. Donzaud, J. Duprat, F. Azaiez, F. Nowacki, H. Grawe, Z. Dombrádi, F. Amorini, A. Astier *et al.*, Phys. Rev. Lett. **88**, 092501 (2002).
[57] N. Bree, I. Stefanescu, P. A. Butler, J. Cederkäll, T. Davinson, P. Delahaye, J. Eberth, D. Fedorov, V. N. Fedosseev, L. M. Fraile *et al.*, Phys. Rev. C **78**, 047301 (2008).

[58] W. Rother, A. Dewald, H. Iwasaki, S. M. Lenzi, K. Starosta, D. Bazin, T. Baugher, B. A. Brown, H. L. Crawford, C. Fransen *et al.*, Phys. Rev. Lett. **106**, 022502 (2011).
[59] B. Crider, C. Prokop, S. Liddick, M. Al-Shudifat, A. Ayangeakaa, M. Carpenter, J. Carroll, J. Chen, C. Chiara, H. David *et al.*, Phys. Lett. B **763**, 108 (2016).
[60] T. Wakasa, K. Ogata, and T. Noro, Prog. Part. Nucl. Phys. **96**, 32 (2017).
[61] Z. Elekes, A. Kripkó, D. Sohler, K. Sieja, K. Ogata, K. Yoshida, P. Doornenbal, A. Obertelli, G. Authelet, H. Baba *et al.* (SunFlower Collaboration), Phys. Rev. C **99**, 014312 (2019).
[62] M. Wang, G. Audi, F. G. Kondev, W. Huang, S. Naimi, and X. Xu, Chin. Phys. C **41**, 030003 (2017).
[63] J. Raynal, Phys. Rev. C **23**, 2571 (1981).
[64] A. Koning and J. Delaroche, Nucl. Phys. A **713**, 231 (2003).
[65] V. R. Brown and V. A. Madsen, Phys. Rev. C **17**, 1943 (1978).
[66] A. Bernstein, V. Brown, and V. Madsen, Phys. Lett. B **103**, 255 (1981).
[67] Z. Elekes, Z. Dombrádi, A. Saito, N. Aoi, H. Baba, K. Demichi, Z. Fülöp, J. Gibelin, T. Gomi, H. Hasegawa *et al.*, Phys. Rev. C **73**, 044314 (2006).
[68] S. Suchyta, S. N. Liddick, C. J. Chiara, W. B. Walters, M. P. Carpenter, H. L. Crawford, G. F. Grinyer, G. Gürdal, A. Klose, E. A. McCutchan *et al.*, Phys. Rev. C **89**, 034317 (2014).
[69] L. Gaudefroy, O. Sorlin, C. Donzaud, J. C. Angélique, F. Azaiez, C. Bourgeois, V. Chiste, Z. Dlouhy, S. Grévy, D. Guillemaud-Mueller *et al.*, Eur. Phys. J. A **23**, 41 (2005).
[70] H. J. Ong, N. Imai, N. Aoi, H. Sakurai, Z. Dombrádi, A. Saito, Z. Elekes, H. Baba, K. Demichi, Z. S. Fülöp *et al.*, Phys. Rev. C **73**, 024610 (2006).
[71] P. Möller, A. Sierk, T. Ichikawa, and H. Sagawa, At. Data Nucl. Data Tables **109–110**, 1 (2016).
[72] K. A. Erb, J. E. Holden, I. Y. Lee, J. X. Saladin, and T. K. Saylor, Phys. Rev. Lett. **29**, 1010 (1972).
[73] S. M. Al-Rawashdeh and M. I. Jaghoub, Eur. Phys. J. A **54**, 62 (2018).
[74] R. De Swiniarski, A. Genoux-Lubain, G. Bagieu, J. Cavaignac, D. Worledge, and J. Raynal, Phys. Lett. B **43**, 27 (1973).
[75] G. Haouat, C. Lagrange, R. de Swiniarski, F. Dietrich, J. P. Delaroche, and Y. Patin, Phys. Rev. C **30**, 1795 (1984).
[76] S. Takeuchi, N. Aoi, T. Motobayashi, S. Ota, E. Takeshita, H. Suzuki, H. Baba, T. Fukui, Y. Hashimoto, K. Ieki *et al.*, Phys. Rev. C **79**, 054319 (2009).
[77] F. Flavigny, A. Obertelli, A. Bonaccorso, G. F. Grinyer, C. Louchart, L. Nalpas, and A. Signoracci, Phys. Rev. Lett. **108**, 252501 (2012).